

A High-Resolution In Vivo Atlas of the Human Brain's Benzodiazepine Binding Site of GABA_A Receptors

Running Title: A High-Resolution Atlas of the Human Brain's BZ binding site of GABA_AR

Martin Nørgaard^{1,2**}, Vincent Beliveau^{5**}, Melanie Ganz^{1,3}, Claus Svarer¹, Lars H Pinborg^{1,2},
Sune H Keller⁶, Peter S Jensen¹, Douglas N. Greve⁴, Gitte M. Knudsen^{1,2*}

¹ Neurobiology Research Unit & CIMBI, Copenhagen University Hospital, Rigshospitalet, Copenhagen, Denmark

² Institute of Clinical Medicine, University of Copenhagen, Copenhagen, Denmark

³ University of Copenhagen, Department of Computer Science, Copenhagen, Denmark

⁴ Athinoula A. Martinos Center for Biomedical Imaging, Massachusetts General Hospital, Harvard Medical School,
Boston, MA, USA

⁵ Medical University of Innsbruck, Department of Neurology, Innsbruck, Austria

⁶ Department of Clinical Physiology, Nuclear Medicine and PET, Rigshospitalet, Copenhagen, Denmark

*** Corresponding author:**

Professor Gitte Moos Knudsen

Neurobiology Research Unit, Section 6931, Rigshospitalet

9 Blegdamsvej

DK-2100 Copenhagen

+45 3545 6720

gmk@nru.dk

**** These authors contributed equally**

ABSTRACT

Gamma-aminobutyric acid (GABA) is the main inhibitory neurotransmitter in the human brain and plays a key role in several brain functions and neuropsychiatric disorders such as anxiety, epilepsy, and depression. The binding of benzodiazepines to the benzodiazepine receptor sites (BZR) located on GABA_A receptors (GABA_ARs) potentiates the inhibitory effect of GABA leading to the anxiolytic, anticonvulsant and sedative effects used for treatment of those disorders. However, the function of GABA_ARs and the expression of BZR protein is determined by the GABA_AR subunit stoichiometry (19 genes coding for individual subunits), and it remains to be established how the pentamer composition varies between brain regions and individuals.

Here, we present a quantitative high-resolution in vivo atlas of the human brain BZR, generated on the basis of [¹¹C]flumazenil Positron Emission Tomography (PET) data. Next, based on autoradiography data, we transform the PET-generated atlas from binding values into BZR protein density. Finally, we examine the brain regional association with mRNA expression for the 19 subunits in the GABA_AR, including an estimation of the minimally required expression of mRNA levels for each subunit to translate into BZR protein.

This represents the first publicly available quantitative high-resolution in vivo atlas of the spatial distribution of BZR densities in the healthy human brain. The atlas provides a unique neuroscientific tool as well as novel insights into the association between mRNA expression for individual subunits in the GABA_AR and the BZR density at each location in the brain.

Key words: GABA, PET, Atlas, Autoradiography, mRNA, benzodiazepine binding site

INTRODUCTION

Gamma-aminobutyric acid (GABA) is the main inhibitory neurotransmitter in the human brain and is a key component in several brain functions and in neuropsychiatric disorders, including anxiety, epilepsy, and depression [1]. The GABA_A receptor (GABA_AR) is a pentameric complex that functions as a ligand-gated chloride ion channel and it is the target of several pharmacological compounds such as anesthetics, antiepileptics, and hypnotics.

Benzodiazepines are well-known for their sedative, anticonvulsive and anxiolytic effects. They act as positive allosteric modulators via the benzodiazepine binding sites (BZR) which are located between the $\alpha_{1,2,3,5}$ and γ_{1-3} subunits in the pentameric constellation of the postsynaptic ionotropic GABA_AR. In total, 19 subunits (α_{1-6} , β_{1-3} , γ_{1-3} , ρ_{1-3} , δ , ϵ , θ , π) have currently been identified, and the constellation of subunits to form GABA_ARs, and consequently the expression of and affinity to the BZR site, has been shown to differ between individuals, between brain regions, and across the life span [1].

High-resolution quantitative human brain atlases of e.g., receptors represent a highly valuable reference tool in neuroimaging research to inform about the in vivo 3-dimensional distribution and density of specific targets. On the basis of high-resolution PET neuroimaging data from 210 healthy individuals, Beliveau et al. 2017 [2] created a quantitative high-resolution atlas of the serotonin system (four receptors, and the serotonin transporter), providing a valuable reference for researchers studying human brain disorders, or effects of pharmacological interventions on the serotonin system that may subsequently down- or upregulate the receptors. Because the functional organization of receptor systems may be different than commonly defined structural organizations (e.g. Brodmann [3]), it is important to define and use the organization of the receptor systems modulating brain function not only to capture a more refined view of the brain [4], but also to provide insights in novel brain parcellations.

Here, we present the first quantitative PET-based high-resolution in vivo 3D human brain atlas of the distribution of BZRs; an atlas to serve as a reference in future studies. Based on autoradiography data, we transform the PET generated atlas into brain regional protein densities of BZR and compare it to the mRNA expression for individual subunits in the GABA_AR, using the Allen Human Brain Atlas [5].

METHODS

Study participants and neuroimaging

Sixteen healthy participants (9 females; mean age \pm SD: 26.6 \pm 8 years, range 19-46 years) were included in the study [6]. The study was approved by the Regional Ethics Committee (KF 01280377), and all subjects provided written informed consent prior to participation, in accordance with The Declaration of Helsinki II. Data from 10 individuals have entered a previous paper (Feng et al. 2016 [7]) where more detailed accounts of the methods can be found. The participants were scanned between 1 and 3 times with the High-Resolution Research Tomograph (HRRT, CTI/Siemens) PET scanner at Rigshospitalet (Copenhagen, Denmark) with the radioligand [¹¹C]flumazenil (26 unique PET scans in total). After an initial transmission scan [8], the radioligand was given either as an intravenous bolus injection or as a bolus-infusion, and a PET emission scan was conducted over 90 minutes, starting at the time of injection. PET data was reconstructed into 35 frames (6x5, 10x15, 4x30, 5x120, 5x300, 5x600 seconds) with isotropic voxels of 1.2 mm using a 3D-ordered subset expectation maximum and point spread function modelling (3D-OSEM-PSF) (16 subsets, 10 iterations) with [¹³⁷Cs]transmission scan-based attenuation correction and no postfiltering [9-11]. Arterial sampling was also performed and the arterial input function was corrected for radiometabolites [7]. The reconstructed PET data were motion corrected using the reconcile procedure in AIR (v. 5.2.5, <http://loni.usc.edu/Software/AIR>),

99 and our criterion for acceptable motion was a median movement less than 3 mm across frames. The
 100 PET tracer injection protocols carried out for each subject are listed in Table S1 in the
 101 supplementary.
 102 An isotropic T1-weighted MP-RAGE was acquired for all participants (matrix size = 256 x 256 x
 103 192; voxel size = 1 mm; TR/TE/TI = 1550/3.04/800 ms; flip angle = 9°) using either a Magnetom
 104 Trio 3T or a 3T Verio MR scanner (both Siemens Inc.). Furthermore, an isotropic T2-weighted
 105 sequence (matrix size 256 x 256 x 176; voxel size = 1 mm; TR/TE = 3200/409 ms; flip angle =
 106 120°) was acquired for all participants. All acquired MRI's were corrected for gradient
 107 nonlinearities [12] and examined to ensure absence of structural abnormalities.
 108 The MR data was processed using FreeSurfer (v.6.0) [13], and co-registered to the PET data using a
 109 rigid transformation and a normalized mutual information cost function.
 110 Regional time-activity curves (TACs) of the target concentration, C_T , were obtained using
 111 PETsurfer [14] defined by the Desikan-Killiany atlas. Voxel-wise TACs in common volume space
 112 (MNI152) were obtained using the Combined Volumetric and Surface (CVS) registration, and
 113 volume smoothed with a 5 mm FWHM Gaussian filter. Surface-based TACs in common space
 114 (fsaverage) were obtained using the cortical-surface registration provided by FreeSurfer and surface
 115 smoothed by a Gaussian filter with 10 mm FWHM [13, 14].

116

117 **Quantification of BZR Availability**

118 The PET data were quantified to estimate total distribution volumes (V_T) for each region using
 119 steady-state analysis for the bolus-infusion experiments and Logan analysis [15] for the bolus
 120 injections, both using the metabolite-corrected plasma curve as input function (Figure S1) [7].

121

122 *Blood Acquisition and Analysis*

For the bolus-infusion experiments, blood sampling was carried out by cannula insertion into one of the cubital veins, while another cannula was inserted to the other cubital vein for radiotracer administration.

For the bolus experiments, arterial blood sampling was carried out by cannula insertion into the radial artery of the nondominant arm. During the first 10 minutes of the PET scan, blood measurements were counted continuously in whole-blood using an ABSS autosampler (Allogg Technology), and three samples were drawn manually to calibrate the autosamples. The plasma to whole-blood ratio was obtained by manually drawing blood samples at 18 time points, measured using a well counter (Cobra 5003; Packard Instruments), and decay-corrected to the time of injection of the radiotracer. For correction of radiometabolites, nine blood samples were drawn during the PET scan and analysed for metabolites using radio-high performance liquid chromatography (HPLC). The metabolite-corrected plasma input function, C_P , was estimated as the product of the parent compound fitted using a biexponential function and the total plasma concentration.

Data Analysis

An overview of the complete analysis workflow can be found in Figure S1 in the supplementary. The metabolite-corrected blood data curves were interpolated to the time points of the PET scan using a cubic spline. All resulting blood curves used for kinetic modeling can be found in the supplementary material.

For bolus-infusion experiments, the plateau for steady-state was used to calculate V_T as an average of the ratio between C_T and C_P from 35 to 80 minutes after the beginning of tracer administration [7]. For the bolus injections, the invasive Logan was used to estimate V_T using the metabolite-corrected input function with $t^*=35$ minutes for all regions and subjects [16].

Since the non-displaceable distribution volume, V_{ND} , is small but not negligible for [^{11}C]flumazenil [16], the outcome of these analyses, V_T , reflects the sum of specific (i.e., BZR) bound distribution volume, V_S , and V_{ND} for all regions, including surface- and voxel maps for all scans. All kinetic models applied in this paper were implemented in MATLAB v. 2016b.

In Vivo Binding and Autoradiography

The conversion from 3D V_T images with the unit ml/cm^3 to BZR density (pmol per gram protein) was done by normalizing regional V_T with the corresponding regional postmortem human brain [^3H]diazepam autoradiography data from Braestrup et al. 1977 [17]. This included 11 brain regions; inferior frontal cortex, inferior central cortex, occipital cortex, temporal cortex, cerebellum, hippocampus, amygdala, thalamus, caudate, putamen and pons. As a linear relationship between the regional average V_T 's across subjects and the corresponding BZR densities could be established, V_{ND} could be estimated from the intercept (Figure 1B). To account for noise in the autoradiography estimates (y-axis), the standard deviation reported in [17] was used to draw random samples from a normal distribution for each region, specified by the region-specific mean and standard deviation. This procedure was repeated 1,000 times, and parameter estimates were fitted for each iteration to obtain an intercept and a slope using a linear model. A subject-specific mean estimate of the slope and intercept was obtained by averaging over the 1,000 estimates (Table S2). Finally, average V_T estimates were obtained by averaging across subjects, and fitted using a linear model to obtain a groupwise association between autoradiography and V_T (Figure 1B). This model was used to convert all surface- and voxel maps into densities of BZR availability (Figure 1A & Figure S1). Units of pmol/g tissue were converted to pmol/ml using a gray matter density of 1.045 g/ml, as done in [2].

171 **In Vivo Binding and mRNA Expression**

172 Regional V_T estimates were compared to mRNA expression values of the 19 subunits of the
 173 GABA_AR obtained using the Allen Human Brain Atlas (AHBA) [5]. The AHBA contains probe
 174 information from 6 human postmortem brains, where each probe provides mRNA levels (log₂
 175 intensity) for all genes and coordinates in MNI152 space. The values from each probe were
 176 matched to a brain region defined by the Desikan-Killiany atlas, and averaged within regions to
 177 provide a regional estimate of mRNA expression for each of the 19 subunits. Further information
 178 can be found in [2].

179 A linear model between the BZR density and the mRNA expression for each of the 19 subunits was
 180 used to examine the correspondence between regions. The intercept (I) was estimated to represent
 181 the minimally required expression of mRNA levels for each subunit to translate into BZR protein.

182

183 **Statistical Analysis**

184 A linear mixed effects model was used to examine the effects of age, sex, administration form
 185 (bolus or bolus-infusion) and multiple scan sessions for a single subject, on the regional estimates
 186 of V_T . The model included age, sex, and the interaction between age and sex as fixed effects. The
 187 administration form (bolus or bolus-infusion) and subjects (i.e. multiple scan sessions for a single
 188 subject) were modeled as random effects. The P-values obtained from each regional analysis (N =
 189 11) were adjusted for multiple comparisons using false-discovery rate (FDR = 0.05).

190 A principal component analysis (PCA) was carried out using the mRNA expression for the 19
 191 subunits and the BZR density for all subcortical and cortical regions (N = 48). Prior to running the
 192 PCA, the data was standardized (mean subtracted and normalized by the standard deviation). All
 193 the data is available in the supplementary material.

194

RESULTS

The regional V_T 's and the postmortem human brain autoradiography were highly correlated (Pearson's $R=0.96$) and the intercept, V_{ND} , was low, on average 0.51 across subjects (range 0.04-1.31) (Figure 1). Using a linear mixed effects model, we found no age or gender related effects on regional estimates of V_T , nor an effect of administration form or multiple scan sessions for a single subject (Table S3). The BZR densities were high in cortical areas (600-1000 pmol/ml), medium in subcortical regions (300-600 pmol/ml), and low in the brainstem (<200 pmol/ml).

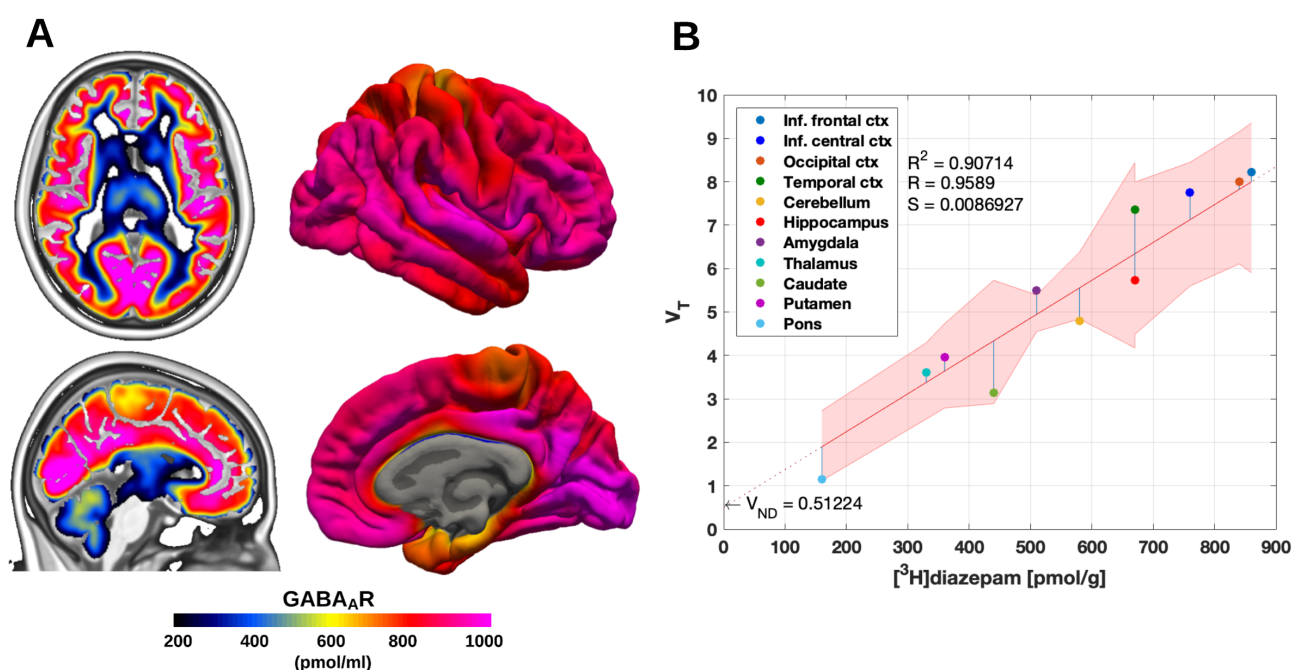


Figure 1: (A) High resolution human brain atlas of GABA_AR density (pmol/ml) in MNI152 space (left) and in fsaverage space (right) (B) Average regional distribution volumes (V_T) and benzodiazepine receptor density for the GABA_AR. The regional V_T 's determined by PET were matched to the corresponding regions from the $[^3H]$ diazepam autoradiography data. The regression is shown as the black line, and the intercept is the non-displaceable distribution volume (V_{ND}). The shaded area is the 95% confidence interval.

The association between BZR densities and mRNA expression showed a medium to high correlation for each of the subunits included in the most common pentameric GABA_AR, i.e., $\alpha_1\beta_2\gamma_2$

212 (48% mRNA expression in the brain [1], Table I) with Pearson's $R > 0.62$ (range: 0.62-0.88,
 213 $P < 0.0001$) for all 3 subunits (Figure 2A-C).
 214 The PCA showed that 6 components explained $>90\%$ of the total variance, with the first and second
 215 component explaining 29.3% and 23.5%, respectively (Figure 2D). The biplot in Figure 2D shows
 216 the contribution of each subunit to the BZR density, indicating a high correlation between the BZR
 217 density and the subunits $\alpha_1, \beta_2, \gamma_2, \gamma_3$, whereas the subunits γ_1, ρ_1 and ρ_3 were negatively correlated
 218 with the BZR density.

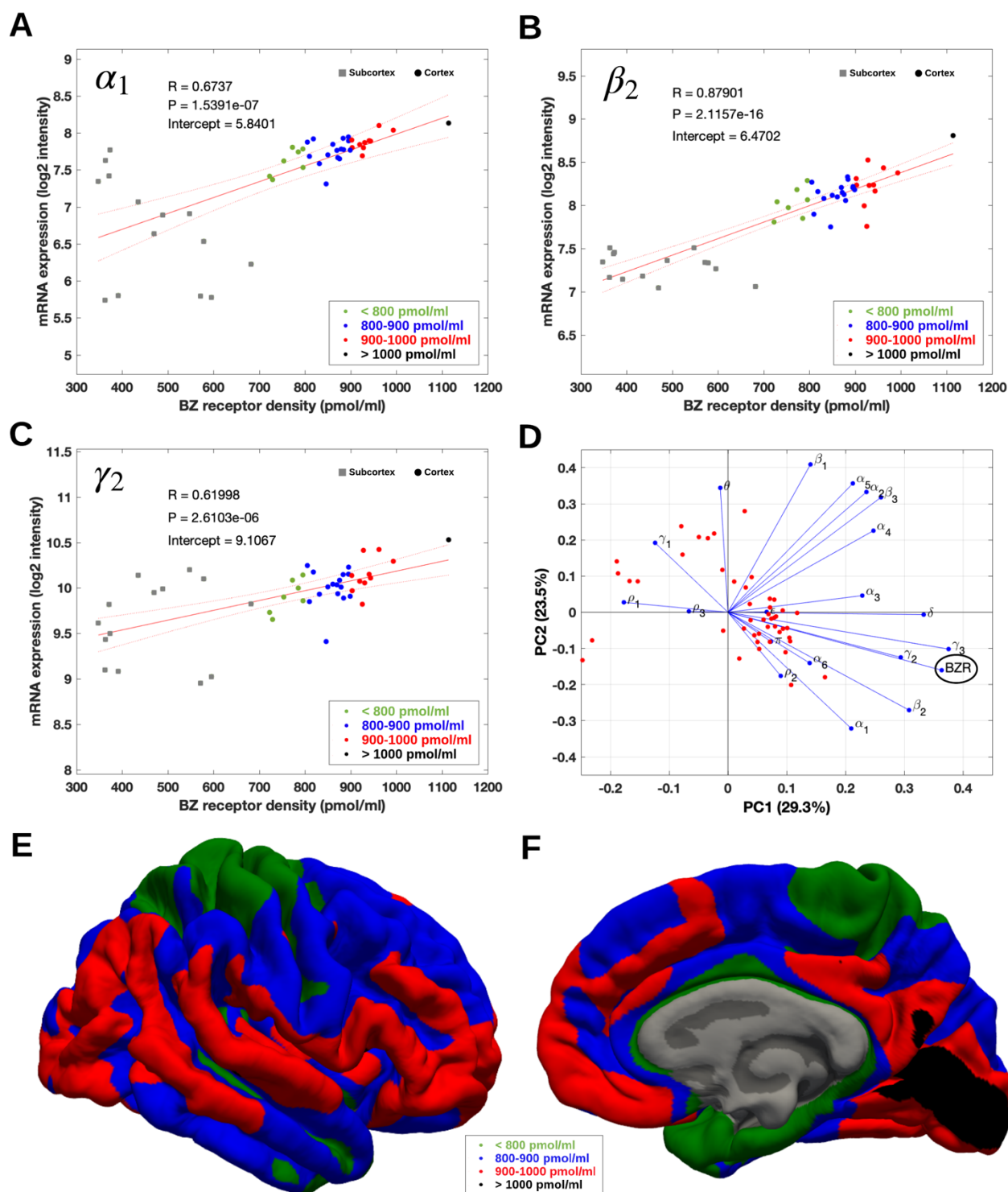


Figure 2: (A-C) Association between mRNA expression (log2 intensity) and BZR density for the subunits of the GABA_AR most commonly represented in the BZR, α_1 in (A), β_2 in (B), and γ_2 in (C). The points are regional estimates for subcortex (squares) and cortex (round dots), and are color coded according to the density, green (< 800 pmol/ml), blue (800-900 pmol/ml), red (900-1.000 pmol/ml), and black (> 1.000 pmol/ml). (D) Biplot of the (scaled) first two principal components (%)

variance explained) of a PCA of the 19 subunits and BZR. (E-F) The spatial distribution of BZR density according to the specified color coding shown on the lateral and medial surface of the brain.

Table I shows the linear association (Pearson's R) between mRNA expression of 14 of the 19 available subunits of GABA_AR and BZR density, ranging between -0.37 (γ_1) and 0.92 (γ_3). Six of the subunits (α_1 , α_3 , β_2 , γ_2 , γ_3 and δ) showed a significant correlation (corrected for multiple comparisons using Bonferroni, $P < 0.01$). The intercept (I) for each of the subunits is the minimal mRNA expression (log2 intensity unit) required for translation into BZR protein and ranged from 1.5 (γ_3) to 9.1 (γ_2). Only the six subunits with a significant association ($P < 0.01$) between mRNA expression and BZR density (α_1 , α_3 , β_2 , γ_2 , γ_3 and δ) were considered to have valid intercepts. The variance explained (V) for each of the subunits was obtained from Sequiera et al. 2019 [1] and shows the proportional contribution (%) from each subunit on the total mRNA expression in the brain across all subunits. Most of the variance was explained by the subunits α_1 , α_2 , β_2 , γ_2 , and δ , contributing with 67% of the variance (Table 1).

	α_1	α_2	α_3	α_4	α_5	α_6	β_1	β_2	β_3	γ_1	γ_2	γ_3	θ	δ
R	0.67	0.28	0.39	0.33	0.15	0.36	0.03	0.88	0.26	-0.37	0.62	0.92	-0.33	0.71
P	<0.01	0.05	<0.01	0.02	0.31	0.01	0.84	<0.01	0.07	0.01	<0.01	<0.01	0.02	<0.01
I	5.8	7.2	5.1	4.9	6.9	1.9	8.5	6.5	7.4	8.2	9.1	1.5	3.2	4.5
V	16	11	2	2	5	3	5	12	7	7	20	0.2	0.2	8

Table I: Association between mRNA subunit expression (log2 units) and benzodiazepine receptor density (pmol/ml) for 14 of the available 19 subunits of the GABA_A receptor, explaining 98.4% of the total variance across brain regions. The associations for the individual subunits are summarized by the Pearson correlation coefficient (R), the uncorrected P-value (P), the intercept (I), and the variance explained (V). The variance explained was obtained from Sequiera et al. 2019 [1].

245 DISCUSSION

246 Here, we present the first quantitative high-resolution in vivo human brain atlas of BZR protein
247 density, freely available at <https://nru.dk/BZR-atlas>. All the data and supplementary information is
248 also publicly available.

249 First, we validated the association between the in vivo BZR protein density and mRNA
250 expression. This validation showed a very strong relationship between [¹¹C]flumazenil-PET and the
251 autoradiography data from Braestrup et al. 1977 [17], supporting the use of [¹¹C]flumazenil-PET as
252 a reliable putative marker for BZR availability in the living human brain.

253 Autoradiography is the gold standard for estimating the density of specific receptors in the brain
254 [17]. Braestrup et al. 1977 [17] used the agonist tracer [³H]diazepam to estimate the density of
255 available BZRs, but despite that [³H]diazepam [18] and the antagonist tracer [¹¹C]flumazenil used
256 in PET [19, 20] have different pharmacological properties, there is no evidence for differences in
257 their ability to bind to other receptors, i.e. they both display low non-specific binding. However,
258 while the non-specific component is often neglected in [¹¹C]flumazenil-PET studies, we observed a
259 minor non-specific component across all subjects and scans that will potentially bias the subject-
260 specific estimate of BZR availability if not taken into account. [¹¹C]flumazenil-PET studies
261 commonly use reference tissue modeling and the pons as reference region for estimation of BZR
262 availability [21]. For all subjects and scans in this study, the V_T in pons was higher than the V_{ND} ,
263 suggesting that this region has specific BZR binding. Therefore, reference tissue modeling of the
264 PET data using pons as a reference region is not entirely valid and may be associated with an
265 underestimation of GABA_AR availability [21].

266 To make our estimates from [¹¹C]flumazenil-PET more comparable to Braestrup et al. 1977 [17],
267 we carried out a post-hoc analysis to estimate the specific binding in the occipital cortex as $V_S =$
268 $(f_p * B_{avail}) / K_D$ [15] using $f_p = 0.04$ [14], $B_{avail} = 880$ pmol/ml, $K_D = 4.8$ nM [17]. This resulted in a V_S

269 equal to 7.3 ml/cm³. This estimate is very close to the average specific binding ($V_s = 7.5$ ml/cm³)
 270 obtained in our PET studies. In comparison, Lassen et al. 1995 [20] used [¹¹C]flumazenil to
 271 estimate the $B_{avail} = 120$ nmol/L, $K_D = 14$ nM, and $BP = B_{avail}/K_D = 8.9$ ml/cm³, based on partial
 272 blocking of the receptor. Several other studies have reported similar or lower B_{avail} and K_D estimates
 273 using PET [22, 23]. However, taking into account the free fraction in plasma of flumazenil ($f_p =$
 274 50%), the specific binding in Lassen et al. 1977 is equal to 4.3 ml/cm³. The estimates by Lassen et
 275 al. 1993 [20] are much lower for both V_s and B_{avail} compared to the estimates obtained in this study
 276 and Braestrup et al. 1977 [17], and is likely the result of limited spatial resolution of the PET
 277 scanner (ECAT 953b; CTI PET Systems, Knoxville, TN, USA) [11], and increased partial volume
 278 effects (PVEs). Nevertheless, by using a high-resolution PET scanner as the HRRT to limit PVEs,
 279 [¹¹C]flumazenil-PET with arterial blood measurements can be used as a reliable putative marker for
 280 BZR availability in the living human brain.

281 The second validation showed a significant association across brain regions between the
 282 expression of mRNA levels for the subunits α_1 , α_3 , β_2 , γ_2 , γ_3 and δ , and the BZR protein density.
 283 Together, these six subunits explain 67% of the total mRNA expression across the brain. The results
 284 confirm previous evidence on the existence of a BZR binding site located between the α_1 and γ_2
 285 subunits in the commonly expressed pentameric GABA_AR subtype $\alpha_1\beta_2\gamma_2$ [24]. We provide novel
 286 evidence of the minimally required expression of mRNA for the translation of BZR proteins for the
 287 α_1 (= 5.8 log2 intensity), β_2 (= 6.5 log2 intensity) and γ_2 (= 9.1 log2 intensity) subunits. Therefore,
 288 an imbalance in the expression of mRNA may have consequences in neuropsychiatric disorders,
 289 with the inability to produce BZR proteins due to reduced expression of mRNA. In general, the
 290 association between mRNA subunit expression and BZR density was particularly high throughout
 291 the neocortex (Figure 2), whereas the associations varied more in the subcortical regions (BZR
 292 density < 700 pmol/ml). The brain region with the highest BZR density was the occipital cortex,

293 which has been documented to be particularly rich in both α_1 and β_2 subunits [1]. The remaining
 294 subunits showed a more variable association between transcription and translation, which might be
 295 caused by regional variations, due to either transport of the subunit protein away from the site of
 296 production or due to non-linear relationships between expression and translation. An indirect
 297 relationship between transcription and translation is not uncommon and has also been observed for
 298 other proteins, e.g., the serotonin transporter and the 5-HT_{2A} receptor [2].

299 Subcortical regions such as the striatum have a high expression of α_4 subunits, and the amygdala
 300 has a high expression of the α_2 , β_1 and γ_1 subunits [1]. In our work, the association between mRNA
 301 expression of the γ_1 subunit and BZR density was found to be negative, consistent with existing
 302 evidence that the expression of β_1 is negatively correlated with the expression of β_2 [1]. Together,
 303 this evidence points toward a reduced BZR density in these regions, likely caused by the
 304 stoichiometry of the subunits to form the GABA_AR. For an in-depth analysis on the subunits only
 305 we refer the reader to Sequiera et al. 2019 [1].

306 Our study is not without limitations. First, the log₂ intensity unit does not directly reflect
 307 quantitative mRNA expression levels, so only the relative differences in mRNA expression are
 308 useful for comparison between subunits.
 309 Second, the association between mRNA and BZR density only allows for a direct comparison
 310 between the individual subunit and BZR density and not their interaction with other subunits. In
 311 addition, it cannot be excluded that different BZR binding pentamers have different affinity for ¹¹C-
 312 flumazenil. For example, it has been shown that flumazenil has a 200-fold higher affinity to
 313 receptors with the configuration α_1 , β_2 and γ_2 , than the affinity to receptors containing the α_6 subunit
 314 [19]. However, as PET acquisitions are carried out using tracer doses (i.e., $\ll K_D$) this should not
 315 impact the estimation of the specific binding of BZRs.

316 In the future, the development of GABA_AR subunit-specific radioligands would be helpful to
 317 examine the GABA-ergic system in more detail. With the addition of such tools, one could gain
 318 even more insight into if pentamer subunit composition affects the affinity to pharmacological
 319 targets and if certain brain disorders are associated with abnormalities in subunit composition of the
 320 GABA_AR.

321

322 CONCLUSIONS

323 This high-resolution in vivo atlas of the spatial distribution of BZR densities in the healthy human
 324 brain provides a highly valuable tool for investigation of the GABA system, e.g., as a reference for
 325 patient groups with alterations in the cerebral GABA system. The findings provide additional
 326 insights into the association between mRNA expression for individual subunits in the GABA_AR and
 327 the BZR density at each location in the brain and may be used to evaluate the efficacy of
 328 pharmacological targets acting on the BZR.

329

330 ACKNOWLEDGEMENTS

331 We wish to thank all the participants for kindly joining the research project. We thank the John and
 332 Birthe Meyer Foundation for the donation of the cyclotron and HRRT scanner used in this study.
 333 Nic Gillings, Bente Dall, and Ling Feng are also greatly acknowledged for their expert
 334 assistance. We also thank the VU University Medical Centre, Amsterdam, Netherlands, for sharing
 335 their knowledge and expertise on [¹¹C]flumazenil.

336 MN was supported by the National Institutes of Health (Grant 5R21EB018964-02), the Lundbeck
 337 Foundation (Grant R90-A7722), and the Independent Research Fund Denmark (DFF-1331-00109 &
 338 DFF-4183-00627). DNG was supported by NIH grant R01EB023281 and R01NS105820.

339

340 **AUTHOR CONTRIBUTIONS**

341 MN, VB and GMK contributed to the design of the work and analyzed the data. MN, VB, MG, CS,
342 SHK, PSJ, LHP, DNG, and MGK interpreted the data. All authors critically reviewed the
343 manuscript and approved the submitted version.

345 **DISCLOSURE/CONFLICT OF INTEREST**

346 GMK has received honoraria as an expert advisor for Sage Therapeutics and as a speaker for Janssen.

348 **SUPPLEMENTARY MATERIAL**

349 Please find attached the supplementary material/data.

351 **REFERENCES**

352 [1] Sequeira, A., Shen, K., Gottlieb, A., & Limon, A. (2019). Human brain transcriptome analysis
353 finds region- and subject-specific expression signatures of GABAAR subunits. *Communications*
354 *Biology*, 2(1), 1–14.

356 [2] Beliveau, V., Ganz, M., Feng, L., Svarer, C., Knudsen, G. M., Fisher, P. M., Ozenne, B., ...
357 Højgaard, L., Knudsen, GM.(2017). A High-Resolution In Vivo Atlas of the Human Brain's
358 Serotonin System. *The Journal of Neuroscience*, 37(1), 120–128.

360 [3] Amunts, K., & Zilles, K. (2015). Architectonic Mapping of the Human Brain beyond
361 Brodmann. *Neuron*, 88(6), 1086–1107.

363 [4] Beliveau, V., Ozenne, B., Strother, S., Greve, D. N., Svarer, C., Knudsen, G. M., & Ganz, M.
364 (2020). The structure of the serotonin system: A PET imaging study. *NeuroImage*, 205(April 2019),
365 116240.
366
367 [5] Hawrylycz, M. J., Lein, E. S., Guillozet-Bongaarts, A. L., Shen, E. H., Ng, L., Miller, J. A., ...
368 Jones, A. R. (2012). An anatomically comprehensive atlas of the adult human brain transcriptome.
369 *Nature*, 489(7416), 391–399.
370
371 [6] Knudsen, G. M., Jensen, P. S., Erritzoe, D., Baaré, W. F. C., Ettrup, A., Fisher, P. M., ...
372 Frokjaer, V. G. (2016). The Center for Integrated Molecular Brain Imaging (Cimbi) database.
373 *NeuroImage*, 124, 1213–1219.
374
375 [7] Feng, L., Svarer, C., Madsen, K., Ziebell, M., Dyssegaard, A., Ettrup, A., ... Pinborg, L. H.
376 (2016). Design of Infusion Schemes for Neuroreceptor Imaging: Application to [11C]Flumazenil-
377 PET Steady-State Study. *BioMed Research International*, 2016.
378
379 [8] Keller SH, Svarer C, Sibomana M. Attenuation correction for the HRRT PET-scanner using
380 transmission scatter correction and total variation regularization. *IEEE Trans Med Imaging*.
381 2013;32: 1611–21.
382
383 [9] Sureau FC, Reader AJ, Comtat C, et al. Impact of image-space resolution modeling for studies
384 with the high-resolution research tomograph. *J Nucl Med*. 2008;49: 1000–8.
385

386 [10] Hong IK, Chung ST, Kim HK, et al. Ultra fast symmetry and SIMD-based projection-
387 backprojection (SSP) algorithm for 3-D PET image reconstruction. IEEE Trans Med Imaging.
388 2007;26: 789–803.

389

390 [11] Mazoyer B, Trebossen R, Deutch R, Casey M, Blohm K. Physical characteristics of the ECAT
391 953B/31: a new high resolution brain positron tomograph. IEEE Trans Med Imaging.
392 1991;10(4):499-504.

393

394 [12] Jovicich J, Czanner S, Greve DN, Haley E, van der Kouwe A, Gollub R, Kennedy D, et al.
395 Reliability in Multi-Site Structural MRI Studies: Effects of Gradient Non-Linearity Correction on
396 Phantom and Human Data. NeuroImage, 2006; 30(2): 436–43.

397

398 [13] Fischl B. FreeSurfer. Neuroimage. 2012 Aug 15; 62(2): 774-781.

399

400 [14] Greve, D. N., Svarer, C., Fisher, P. M., Feng, L., Hansen, A. E., Baare, W., ... Knudsen, G. M.
401 (2014). Cortical surface-based analysis reduces bias and variance in kinetic modeling of brain PET
402 data. NeuroImage; Vol. 92; pp. 225–236.

403

404 [15] Logan J, Fowler JS, Volkow ND, Wang GJ, Ding YS, Alexoff DL: Distribution volume ratios
405 without blood sampling from graphical analysis of PET data. J Cereb Blood Flow Metab 1996,
406 16(5):834-840.

407

408 [16] Magata Y, Mukai T, Ihara M, Nishizawa S, Kitano H, Ishizu K, Saji H, Konishi J. Simple
409 analytic method of ¹¹C-flumazenil metabolite in blood. J Nucl Med 2003; 44: 417-421.

410

411 [17] Braestrup, C., Albrechtsen, R., & Squires, R. (1977). High densities of benzodiazepine
412 receptors in human cortical areas. *Nature*, 269(October), 702–704.

413

414 [18] Videæk, C., Friberg, L., Holm, S., Wammen, S., Foged, C., Andersen, J. V., ... Lassen, N. A.
415 (1993). Benzodiazepine receptor equilibrium constants for flumazenil and midazolam determined in
416 humans with the single photon emission computer tomography tracer [123I]iomazenil. *European*
417 *Journal of Pharmacology*, 249(1–2), 43–51.

418

419 [19] Whitwam, J. G., & Amrein, R. (1995). Pharmacology of flumazenil. *Acta Anaesthesiologica*
420 *Scandinavica*, 39(10), 3–14.

421

422 [20] Lassen, N. A., Bartenstein, P. A., Lammertsma, A. A., Pevett, M. C., Turton, D. R., Luthra, S.
423 K., ... Vanggaard Andersen, J. (1995). Benzodiazepine receptor quantification in vivo in humans
424 using [11C]flumazenil and PET: Application of the steady-state principle. *Journal of Cerebral*
425 *Blood Flow and Metabolism*, 15(1), 152–165.

426

427 [21] Klumpers UMH, Boellard R, Veltman DJ, Kloet RW, Hoogendijk JG, Lammertsma AA.
428 Parametric [11C]flumazenil images. *Nuclear Medicine Communications* 2012, 33:422-430.

429

430 [22] Blomquist G, Pauli S, Farde L, Eriksson L, Persson A, Halldin C (1990) Maps of receptor
431 binding parameters in the human brain-a kinetic analysis of PET measurements. *Eur J Nucl Med*
432 16:257-265.

433

- 434 [23] Price JC, Mayberg HS, Dannals RF, Wilson AA, Ravert HT, Frost JJ (1991) Estimation of
 435 benzodiazepine receptor binding parameters using ILC-flumazenil and PET: equilibrium and kinetic
 436 methods. J Cereb Blood Flow Metab 11(Suppl 2):S612
 437
- 438 [24] Zhu, S., Noviello, C. M., Teng, J., Walsh, R. M., Kim, J. J., & Hibbs, R. E. (2018). Structure of
 439 a human synaptic GABAA receptor. Nature, 559(7712), 67–88.